Effect of Dynamical Diffraction in X-Ray Fluorescence Scattering

BORIS W. BATTERMAN
Bell Telephone Laboratories, Murray Hill, New Jersey
(Received 21 August 1963)

With a conventional double-crystal spectrometer, we have obtained direct evidence for the formation of the two types of standing-wave fields formed within the crystal during the diffraction process. As a germanium crystal was rotated through the Bragg-reflection region the fluorescence scattering as well as the diffracted beam was measured. The reflected beam gives the expected Darwin-Prins curve, while the fluorescence curve (a dip at the Bragg angle), is asymmetric with a long tail on the low-angle side. The fluorescence, in this case, is used as a measure of the electric-field intensity at the atomic electrons, and the asymmetry implies that there is less x-ray intensity in the diffracting planes of atoms at low glancing angles than there is at high angles. This is consistent with the dynamical theory prediction of the formation of a nodal plane of the x-ray wave field at the atoms at low glancing angles and an antinode at high angles. We show that the antinode forming at the high-angle side can produce a marked enhancement of the fluorescences over that produced when no diffraction is taking place. Very good agreement between experimental fluorescence intensities and that predicted by dynamical theory was obtained.

INTRODUCTION

IF one Bragg diffracts perfectly collimated and monochromatic x rays from the face of a perfect crystal so that the reflected beam exits the crystal from the same face it enters (Bragg case), the intensity diffracted as a function of angle is the familiar Darwin curve. This is a top-hat curve which includes a range of total reflection typically the order of several seconds of arc. If the crystal is absorbing, the curve is somewhat rounded off, giving a region of almost total reflection and is now asymmetric with less intensity on the high-angle side of the peak. The shape and intensity of these peaks have been experimentally[1–4] verified and checked with theory.

The dynamical theory of diffraction predicts not only the energy reflected by the crystal, but gives a detailed description of the distribution of this energy inside the crystal with respect to the scattering planes of atoms.

Detailed experimental observations in the Bragg case have been carried out by Borrmann and coworkers[4] and more recently by Bonse,[5] who measured the weak intensity transmitted through a thin crystal diffracting in the symmetric Bragg case, and by Authier,[6] who measured the beam leaving the lateral face of the crystal perpendicular to the diffracting face.

In the present experiment we have attempted to check predictions of the theory concerning the distribution of x-ray intensity between the atomic planes. The present method[7] is novel in that we use not the diffracted energy, but the fluorescence radiation of a diffracting atom to measure the dynamical effects in the crystal. The photoelectric absorption at an atom is proportional to the electric-field intensity seen by its absorbing electrons. Therefore, it follows that the fluorescence emitted in conjunction with the diffraction process will directly indicate the changing field intensity at the atomic planes as a function of Bragg angle.

Of the available experimental possibilities, there appears to be a unique combination. Two important conditions to be met are that the crystal must be structurally perfect from the x-ray standpoint, and at the same time must be of a high enough atomic number so that its fluorescence can escape from the crystal and be readily detected by conventional means. Germanium is a unique crystal in that it is readily available in a highly perfect state, and its K fluorescence edge at 1.12 Å is readily excited by Mo K_α radiation of 0.71 Å.

EXPERIMENTAL

The experimental arrangement (Fig. 1) is basically that of a conventional double-crystal spectrometer with a few modifications. The first crystal diffracting the (220) of Mo K_α is asymmetrically cut [(220) planes making an angle of 8° with the surface], and arranged so that the diffracted beam makes the smaller glancing angle with the surface (approximately $2\frac{1}{4}°$). We take advantage of the fact first shown by Renninger[8] that such an asymmetric arrangement will reduce the intrinsic reflection width of the first crystal by a factor of approximately $\sin(\theta-\alpha)/\sin(\theta+\alpha)$, where α is the angle between the lattice planes and the crystal surface. For the 8° asymmetry this corresponds to a reduction factor of about 12.

This now allows the instrument to trace out very nearly the intrinsic reflection properties of the second crystal, and avoids the necessity of convoluting two theoretical curves to make a comparison with the experimental results. Three NaI thallium-doped scintillation counters were used as detectors. One counter (wide open face) set as close as possible to the face of the

[1] M. Renninger, Z. Krist. **89**, 344 (1934).
[2] M. Renninger, Acta Cryst. **8**, 597 (1955).
[3] B. W. Batterman, J. Appl. Phys. **30**, 508 (1959).
[4] G. Borrmann, Naturwiss. **38**, 330 (1951); Z. Physik **142**, 406 (1955); H. Hildebrandt, Z. Krist. **112**, 340 (1959); H. Wagner, Z. Physik **146**, 127 (1956).
[5] U. Bonse, Z. Physik **161**, 310 (1961).
[6] A. Authier, J. Phys. Radium **23**, 961 (1962).
[7] A preliminary report was given in Appl. Phys. Letters **1**, 68 (1962).
[8] M. Renninger, Z. Naturforsch. **16a**, 1110 (1961).

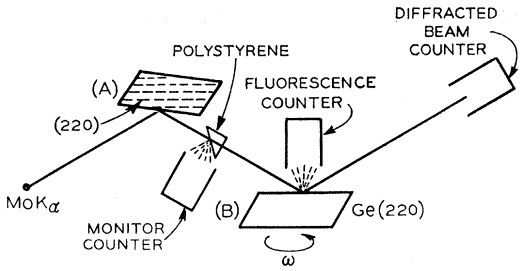

FIG. 1. Parallel arrangement of double-crystal spectrometer with asymmetrically cut first crystal.

second crystal was set to count germanium K fluorescence. Since the energy difference between Mo K_α and Ge K is relatively large, any higher energy molybdenum radiation scattered into the counter could be discriminated against electronically. Another counter set at the correct 2θ position could simultaneously record the diffracted beam. The counter placed in front of the slit between the two crystals acted as a monitor counter for precise measuring of the fluorescence versus angular position of the crystal. The Mo target tube was run at 40 kV and 25 mA. In a typical run the outputs of both the diffracted beam and fluorescence counters were chart-recorded as the crystal was rotated with uniform angular velocity through the range of reflection.

QUALITATIVE RESULTS

In Fig. 2 are the direct chart records of the fluorescence and reflected beam counters. It is apparent that both curves are asymmetric. The reflected beam has lower intensity on the high-angle side of the reflection in agreement with the theoretical Darwin-Prins curve. The fluorescence curve at the reflecting position shows a large dip, to about $\frac{1}{4}$ of the initial value, and has a long tail on the low-angle side which has still not reached the background fluorescence at some 10 peak half-widths from the center of the range of reflection.

The asymmetry in the fluorescence curve is not a result of the asymmetrically cut first crystal. In our initial experiments[7] the curve was quite similar to Fig. 2, even though both crystals were symmetrically cut and the reflection curve was the symmetric convolution of two Darwin-Prins curves. The fluorescence asymmetry is a direct result of the dynamical interaction of the x-ray wave field and atomic planes, and can be explained in a qualitative way as follows: We divide the ideal Darwin curve into three regions, the low- and high-angle tails, called (1) and (3), respectively, and the central region of total reflection, (2). According to dynamical theory, in region (1) the primary and diffracted rays interact to form a wave field which produces a diminution of intensity in the atom planes. When the diffracted wave is strongest and equal to the primary wave at the (1)–(2) boundary, a node exists at the atoms. The situation is similar in the high-angle tail except that there is an enhancement of intensity at the atoms leading to an antinode at the (2)–(3) boundary. Thus, in the tail regions where most of the incident energy is absorbed in the crystal (the reflected intensity is small), the effective linear absorption coefficient is smaller than the normal value in (1) and larger than this in (3). Hence, for the tail regions, the primary beam will be absorbed in a greater depth in (1) than in (3). Since the fluorescence is the result of this absorption, it will be weaker when it exits the surface in region (1) because of a larger self-absorption due to the longer crystal path it must travel to get out. In region (3) there is less self-absorption because, due to the antinode formation at the atoms, the fluorescence is created nearer the surface. In the central region, the large fluorescence dip is merely a result of energy conservation. Here the reflected beam is quite strong and consequently little energy enters the crystal to produce fluorescence. In fact, Fig. 2 shows that the dip is almost a mirror reflection of the diffracted beam. The dominant factor in determining the fluorescence in (2) is the energy allowed to enter the crystal.

In a qualitative way, we have shown that the asymmetric fluorescence curve is a direct result of the two types of wave fields predicted by the dynamical theory. In the next sections we investigate this wave field quantitatively and explain physically some of the details of the fluorescence curve.

QUANTITATIVE THEORY

The fluorescence scattering received at the detector as a function of angle of incidence is determined by the absorption coefficient $\mu(\eta)$ of the wave field inside the crystal, where η, to be defined later, is proportional to the glancing angle of the incident beam. η is included here to emphasize the fact that the absorption of x rays now depends upon the diffraction conditions. The amount of K fluorescence of a germanium atom will be

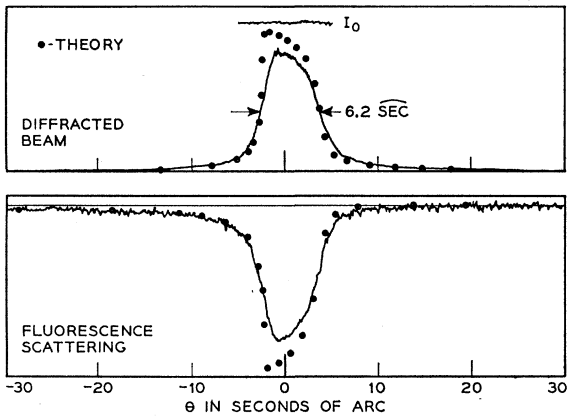

FIG. 2. Chart recordings of fluorescence and diffracted beam counters. The theory points have a single scaling factor. For the diffracted beam the match is made at I_0, the primary beam intensity, while the fluorescence curve is matched at the horizontal tails.

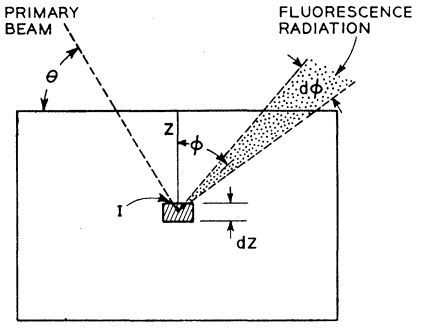

FIG. 3. Volume element used to compute the fluorescence leaving the crystal.

proportional to $\mu(\eta)$ which represents loss per unit length, even though some of the incident energy loss is converted to higher shell fluorescence, Compton x rays, and phonon scattering.

Conservation of energy demands that the energy absorbed in the crystal is proportional to $(1-R^2)$, where R^2 is the ratio of energy in the diffracted beam to the incident beam and is therefore the Darwin-Prins reflection curve. The energy I, reaching a depth Z (Fig. 3), is thus proportional to $(1-R^2)e^{-\mu Z(\eta)Z}$, where $\mu_Z(\eta)$ is the dynamical absorption coefficient with respect to the normal to the crystal surface. We can therefore write for the energy loss between Z and $Z+dZ$,

$$dI \approx (1-R^2)\mu_Z(\eta)e^{-\mu Z(\eta)Z}dZ.$$

A large fraction of this energy will produce K fluorescence distributed equally in all directions. That fraction sent in the conical volume element shown in Fig. 3 is $\frac{1}{2}\sin\varphi d\varphi$ which, upon reaching the crystal surface, has been attenuated by an additional factor of $e^{-\mu_f Z \sec\varphi}$, where μ_f is the linear absorption coefficient of the fluorescence radiation; i.e., Ge K_α or K_β. It follows that the total fluorescence leaving the crystal in any angular range φ_1 to φ_2 for a given incidence angle η is

$$I_f(\eta)=C\frac{(1-R^2)}{2}\mu_Z(\eta) \times\int_0^\infty\int_{\varphi_1}^{\varphi_2} e^{-\mu Z(\eta)Z}e^{-\mu_f Z\sec\varphi}\sin\varphi d\varphi dZ, \quad (1)$$

where C is a proportionality constant. If we define

$$X=\mu_f/\mu_Z(\eta), \quad (2)$$

Equation (1) integrates to

$$I_f(\eta)=C\frac{1-R^2}{2}\left[\cos\varphi_1-\cos\varphi_2+X\ln\frac{X+\cos\varphi_2}{X+\cos\varphi_1}\right]. \quad (3)$$

The total fluorescence leaving the upper surface ($\varphi_1=0$ to $\varphi_2=\pi/2$) is

$$I_f(\eta)=C\frac{1-R^2}{2}\left[1+X\ln\left(\frac{X}{1+X}\right)\right]. \quad (4)$$

If $\mu_f=0$; i.e., there is no loss of fluorescence due to self-absorption, (4) reduces to $C(1-R^2)/2$ which simply states that the shape of the fluorescence curve is the complement of the Darwin-Prins curve.

The angles φ_1 and φ_2 are determined strictly from the acceptance range of the scintillation detector. For the experimental arrangement in Fig. 1 which gave the curves in Fig. 2, $\varphi_1=0$ and $\varphi_2=40.5°$.

To evaluate (3) from theory we need R^2 and the dynamical absorption coefficient $\mu(\eta)$. According to dynamical theory,[9] for the symmetric Bragg case, the wave field inside the crystal for a given angle of incidence can be expressed as two plane waves traveling with amplitude $\mathbf{D}_0$ in the primary beam direction (very nearly) and $\mathbf{D}_H$ in the diffracted beam direction:

$$\mathfrak{D}_0=\mathbf{D}_0\exp(-2\pi iK_0'\cdot\mathbf{r})\exp(-4\pi K_0''\cdot\mathbf{r}), \quad (5a)$$

$$\mathfrak{D}_H=\mathbf{D}_H\exp(-2\pi i\mathbf{K}_H'\cdot\mathbf{r})\exp(-4\pi\mathbf{K}_0''\cdot\mathbf{r}). \quad (5b)$$

The complex wave vector $\mathbf{K}=\mathbf{K}'-i\mathbf{K}''$ includes the absorptive term due to the imaginary part, $-\mathbf{K}_0''$, which is the same for both waves. To arrive at the fluorescence produced by the wave field of Eq. (5a) and (5b), we must explicitly evaluate the damping term $\exp(-4\pi\mathbf{K}_0''\cdot\mathbf{r})$ or, in particular, the complex part of the wave vector, $-\mathbf{K}_0''$.

The complex equation defining the dispersion surface is [see James' Eq. (8.35)]

$$\xi_0\xi_H=\tfrac{1}{4}k^2P^2\Gamma^2F_H\bar{F}_H, \quad (6)$$

where F_H and $\bar{F}_H$ are the structure factors of reflections (hkl) and $(\bar{h}\bar{k}\bar{l})$, respectively, $(F_H=F_H'+iF_H'')$, $\Gamma=(e^2/mc^2)\lambda^2N/\pi$, $P=1$ or $\cos2\theta$ for the σ and π states of polarization, N is the number of unit cells per unit volume, and $k=1/\lambda$. The real part of the dispersion surface with the crystal surface oriented for the symmetric Bragg case and one state of polarization is shown in Fig. 4 in terms of the real coordinates ξ_0' and ξ_H'.

For the real parts, the ξ represents the difference between the actual wave vectors $\mathbf{K}_0'$ and $\mathbf{K}_H'$associated with the tie point A and the vacuum wave vector $\mathbf{k}$ corrected for the average index of refraction; i.e., $k(1-(1/2)\Gamma F_0')$. For the complex treatment it can be

[9] The theory, as presented in this section, cannot easily be expressed in terms of notation and equations which can be referred to a single source. An up-to-date treatment of the theory is in the process of being published. To fill in the gaps in the present treatment, we shall refer to the material in Chap. 8 of R. W. James' *The Optical Principles of the Diffraction of X-Rays* (G. Bell and Sons, London, 1950). The equations quoted in this paper will be expanded or modified forms of those in James' book.

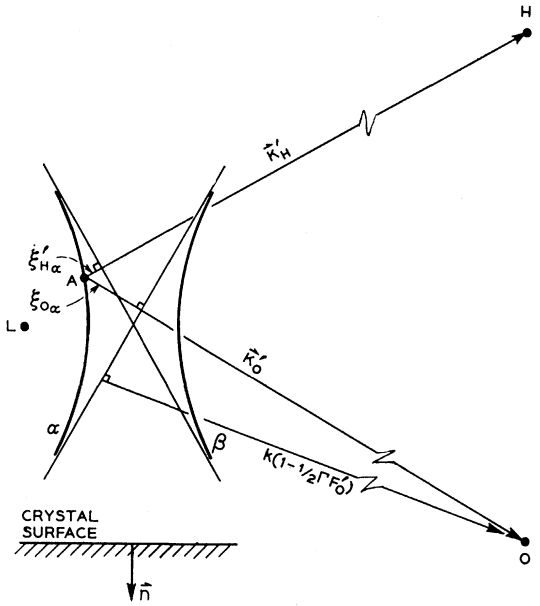

FIG. 4. Dispersion surface oriented for symmetric Bragg reflection.

shown that

$$2k\xi_0=(\mathbf{K}_0\cdot\mathbf{K}_0)^{1/2}-k[1-(1/2)\Gamma F_0], \quad (7a)$$

$$2k\xi_H=(\mathbf{K}_H\cdot\mathbf{K}_H)^{1/2}-k[1-(1/2)\Gamma F_0], \quad (7b)$$

where $\mathbf{K}$ and F_0 are complex quantities. The complex part of the inside wave vector $-\mathbf{K}_0''$, is a vector perpendicular to the incident surface of the crystal since planes of constant absorption are parallel to this surface. It follows from this and Eqs. (7a) and (7b) that

$$K_0''=[-\xi_0''+(1/2)k\Gamma F_0'']/\gamma_0, \quad (8)$$

where γ_0 is the direction cosine of the incident beam with respect to the inward surface normal. We have, in evaluating the square root in (7), treated $|K_0''|/|K_0'|$, which is typically the order of 10^{-6} as a second-order quantity. For the symmetric Bragg case

$$\xi_0=(1/2)k|P|\Gamma(F_H\bar{F}_H)^{1/2}[\eta\pm(\eta^2-1)^{1/2}], \quad (9)$$

where

$$\eta=\frac{-\Delta\theta\sin2\theta+\Gamma F_0}{\Gamma|P|[F_H\bar{F}_H]^{1/2}}=\eta'+i\eta''. \quad (10)$$

The complex Eqs. (9) and (10) can be obtained with some algebra by combining Eqs. (8.39), (8.46), and (8.47) in James.[9]

Since $-\mathbf{K}_0''$ is normal to the crystal surface we have from Eq. (5)

$$4\pi K_0''=\mu_Z(\eta). \quad (11)$$

Inserting the complex part of (9) in (8), and using the fact that the normal linear absorption coefficient is

$$\mu_0=2\pi k\Gamma F_0'', \quad (12)$$

we have finally for $\mu_Z(\eta)$

$$\mu_Z(\eta)=\frac{\mu_0}{\gamma_0}\left[1-|P|\ \mathrm{Im}\left\{\frac{F_H}{F_0''}[\eta\pm(\eta^2-1)^{1/2}]\right\}\right], \quad (13)$$

where Im signifies the imaginary part of the argument. Equation (13) is valid for a centrosymmetric crystal where $F_H=\bar{F}_H$, and where the crystal surface is parallel to the diffracting planes.

The reflection coefficient $R^2=|D_H/D_0|^2$ can be expressed simply [James[9] (8.60)] in terms of a complex η,

$$R^2=|\eta\pm(\eta^2-1)^{1/2}|^2. \quad (14)$$

Since (F_0''/F_H') for the 220 reflection of germanium is the order of (0.07), we can simplify expression (10) for η by neglecting squares of this quantity in comparison to unity, giving

$$\eta'=(-\Delta\theta\sin2\theta+\Gamma F_0')/|P|\Gamma F_H', \quad (15a)$$

$$\eta''=(1/|P|)(F_0''/F_H')(1-\eta'\epsilon|P|), \quad (15b)$$

where $\epsilon=F_H''/F_0''$ is the angular dependence of the imaginary part of the structure factor.

In the present experiment there are four separate fluorescence sources and hence four values of $I_f(\eta)$ at each position η. The σ and π polarization states are absorbed differently because $|P|$ is a part of η, and each of these states produces both Ge K_α and Ge K_β radiation. The combined $I_f(\eta)$ is now proportional to

$$I_f(\eta)\approx I_f^\sigma(K_\alpha)+|\cos2\theta|I_f^\pi(K_\alpha)+\beta(I_f^\sigma(K_\beta)+|\cos2\theta|I_f^\pi(K_\beta)), \quad (16)$$

where β is the relative intensity of the Ge K_α to the Ge K_β fluorescences. (The $|\cos2\theta|$ term results from polarization by the first crystal.)

The absorption coefficients of Mo K_α, Ge K_α, and Ge K_β were experimentally determined in thin single crystals of germanium using a fluorescence spectrometer as the x-ray source. The ratio β was determined by directly measuring the intensities of the K_α to K_β for a thin specimen of germanium powder. A summary of the parameters necessary for the calculation of R^2 and I_f is given in Table I.

For a given value of η' between -50 to $+50$, Eq. (15b) was evaluated for η''. R^2 is then directly de-

TABLE I. Experimental and theoretical constants used to calculate fluorescence scattering. The mass-absorption coefficients refer to the stated wavelength in germanium.

μ_ρ(Mo K_α)	59.9 cm²/g
μ_ρ(Ge K_α)	37.2 cm²/g
μ_ρ(Ge K_β)	27.8 cm²/g
ϵ	0.964[a]
f_0(Ge 220)	23.82[b]
β	0.143

[a] This value was obtained from H. Wagenfeld, J. Appl. Phys. **33**, 2907 (1962), using a Debye temperature of 290°K.
[b] A. J. Freeman, Acta. Cryst. **12**, 929 (1959).

termined from (14) using the algebraic sign for each of the three ranges ($\eta'<-1$, $-1<\eta'<+1$, $\eta'>1$) such that R^2 is always less than unity. Similarly, for each η', $\mu_Z(\eta)$ is calculated according to (13) which gives an I_f [Eq. (4)] for each polarization and each of the two K-emission lines. The I_f were then summed according to (16) to give the expected fluorescence curve.

The points in Fig. 2 are the results of the theoretical computation. The angular width of the theoretical curve is directly determined from Eq. (15a). The only adjustable parameters are the vertical scale factor and the horizontal position of the curve. It can be seen that the agreement in the tail regions is quite good. The long tail at the low-angle side is accurately matched as well as the relatively abrupt rise to the fluorescence background at the high-angle side. The agreement is not as good in the central region where strong diffraction is taking place. This is due to a combination of effects. Because of the sharpness with respect to reflection angle, broadening due to the first crystal, misalignment of the two crystals, and any intrinsic crystalline imperfection would be most pronounced in this region, and would tend to reduce the reflection coefficient and broaden the curves.

FURTHER RESULTS AND DISCUSSION

One interesting feature of the fluorescence curve is the large angular range necessary for the low-angle tail to approach background. This is somewhat surprising since the reflection curve has approached its background considerably closer to the peak. Since details of the reflection and fluorescence curves are intimately connected with the diffraction process it is at first surprising that the diffracted beam has gone essentially to zero and yet the fluorescence has not yet reached the value expected for no diffraction.

In Fig. 5 we give a more detailed measurement of the tail regions of the fluorescence curve. The data are point counts relative to the monitor counter for a given angle of incidence. To reduce drift errors, several measurements at each point were made with the angle repeatedly reset relative to the center of the diffraction curve. The estimated precision for each point is $\pm 0.15\%$. The theoretical curve was fitted as in Fig. 2. Note the expanded vertical scale in Fig. 5. Most of the fluorescence in this figure corresponds to the very weak

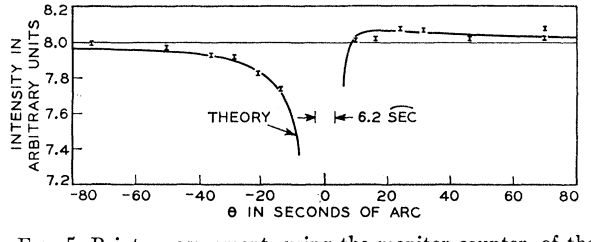

FIG. 5. Point measurement, using the monitor counter, of the tail regions in Fig. 2. The nominal errors for the data points are $\pm 0.15\%$. The solid curve is theory.

tails of the diffracted beam. We see again a rather good fit with theory and definite proof of the very long tail on the low-angle side.

The physical reasons for this tail are made clear if one calculates the field intensity in the atomic planes. If we neglect the damping term in Eqs. (5a) and (5b), the total electric displacement in the crystal is $\mathbf{D}_0+\mathbf{D}_H=\mathbf{D}$ and the intensity proportional to $\mathbf{DD}^*$. Thus,

$$\mathbf{D}^2=|\mathbf{D}_0+\mathbf{D}_H|^2=|\mathbf{D}_0|^2 +|\mathbf{D}_H|^2+\mathbf{D}_0\cdot\mathbf{D}_H\cos 2\pi(x/d)\,, \quad (17)$$

where we have used Bragg's law in the form $\mathbf{K}_H'-\mathbf{K}_0'=\mathbf{H}$, where $|\mathbf{H}|=(d\text{ spacing})^{-1}$ and x is distance normal to the diffracting planes. For the (220) reflection measured here, all the atoms scatter in phase, and the complex phase of the amplitudes $\mathbf{D}_0$ and $\mathbf{D}_H$ will be such as to form nodes or antinodes at the atomic planes (i.e., where $x=0,\ d,\ 2d\cdots$) so that (17) becomes for the σ polarization

$$\mathbf{D}^2=(\mathbf{D}_0^2+\mathbf{D}_H^2)\left[1\pm\frac{2|\mathbf{D}_H|/|\mathbf{D}_0|}{1+(\mathbf{D}_H/\mathbf{D}_0)^2}\cos 2\pi\frac{x}{d}\right]. \quad (18)$$

At the exact Bragg angle, $|D_H|=|D_0|$ and there will be a node or antinode ($\pm$ sign) at the planes. (For the π polarization, no zero node will exist because the coefficient of the cosine will have a factor of $\cos 2\theta$.) The boundary conditions of the problem are such that the amplitudes of the internal waves equal that of the external waves so the $|D_H/D_0|^2$ is just the ratio of primary to diffracted energies, or R^2 in Eq. (14). That portion of (18) which gives the intensity at the atoms and hence determines the emitted fluorescence is therefore proportional to

$$1\pm 2R/(1+R^2)\,. \quad (19)$$

It is easy to see from (19) why the diffracted energy goes to zero much faster than the fluorescence goes to its background. Suppose that the glancing angle corresponds to a reflected intensity of only 1%; i.e., $R^2=0.01$. It follows from (19), that the intensity at the atoms is approximately proportional to (1 ± 0.2) for the two branches whereas if no diffraction took place it should be proportional to unity. The crux of the matter is that the diffracted energy is proportional to the square of the amplitude while the intensity modulation at the atoms goes only as the amplitude. Thus, the reflected energy can be very small while the energy at the atoms departs considerably from the value when the reflected energy is zero, and a long fluorescence tail is to be expected.

It became clear in the course of the computation that the depression or enhancement of the fluorescence in the tails was a function of the acceptance cone angle of the monitor counter. This can be illustrated in Fig. 6. Point A represents some average depth of penetration of the incident beam for the wave field tending to

produce an antinode at the atom [the high-angle region (3)] and B the corresponding point for the nodal field in region (1). A therefore corresponds to a glancing angle $\theta_0+\Delta\theta$ and B to $\theta_0-\Delta\theta$, where θ_0 corresponds to the glancing angle of the center of the diffraction region. The relative value of the fluorescence intensity leaving the crystal in direction φ from the two tail regions is $e^{-\mu f(t_A-t_B)}$. It is clear that as φ increases, that is, as the fluorescence path in the crystal increases, this ratio will increase. As φ approaches 90°, the difference in the fluorescence from corresponding $\Delta\theta$ points in regions (1) and (3) will be enhanced. This suggested putting the fluorescence counter as indicated in Fig. 6 so as to accept that small amount of fluorescence that travels the greatest distance inside the crystal. Although the intensity would be considerably reduced this way, more detail is to be expected in the curve. An experimental curve is shown in Fig. 7. The asymmetry in the fluorescence has been enhanced greatly now, even to the point where we clearly see an enhanced fluorescence on the high-angle side. This results because the origin of the fluorescence is now closer to the surface than when the crystal is not diffracting. Because of the small acceptance angle at the counter and the larger self-absorption of the fluorescence, the intensity is about a factor of 100 smaller than that in Fig. 2 and includes a relatively larger fraction of spurious radiation. We have computed the theoretical fluorescence according to Eq. (16) to leave the crystal between $\varphi_1=85°$ and $\varphi_2=90°$; i.e., radiation leaving within 5° of the crystal surface. These are given by the points in Fig. 7. A single scaling parameter for the intensity was used to match the curves relative to the fluorescence at large angle. The theoretical curve was then translated so that the asymptotic value was the same as the experimental one. The agreement between theory and experiment is excellent. The theoretical curves were also computed for the $\varphi_1-\varphi_2$ angular ranges 80° to 90° and 88.5° to 90°.

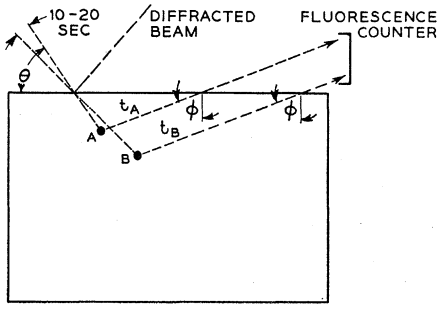

FIG. 6. Ray paths for two beams, one on each side of the actual Bragg angle. The higher angle ray A suffers a greater than normal absorption and hence creates its fluorescence closer to the crystal surface than the low-angle ray B.

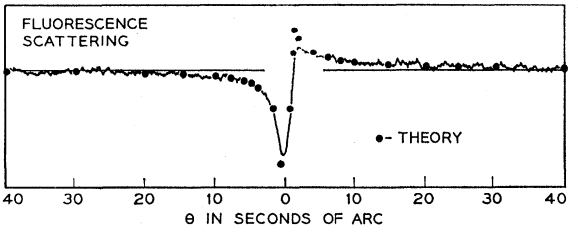

FIG. 7. Fluorescence curve with the counter arranged as in Fig. 6 to accept only the fluorescence making a small angle with the crystal surface. The theory points are computed from Eqs. (3) and (16), with $\varphi_1=85°$ and $\varphi_2=90°$.

These curves have substantially the same shape as the one plotted in Fig. 7 for the tail regions. The only differences occur in the narrow region of the peak and dip where the crystal is diffracting strongly.

SUMMARY AND CONCLUSION

We have used the fluorescence radiation leaving the crystal during a diffraction process as a probe to measure the x-ray wave field inside the crystal. The fluorescence curves show explicit effects due to the two types of standing x-ray wave fields corresponding to the two branches of the dispersion surface. The shape of the fluorescence curve was shown to agree very well with the dynamical theory.

The fluorescence measurement in symmetric Bragg reflection shows up all the basic features of the dispersion surface. As opposed to the thick crystal Borrmann effect where only one branch is active, the reflection experiment traces out the motion of a tie point from one branch to the other, and includes the imaginary solution between the two branches leading to the damped wave in the crystal. For this reason, the fluorescence measurement might prove valuable from a pedagogical standpoint.

This fluorescence experiment using x rays is similar to a neutron diffraction work performed by Knowles[10] who investigated an enhanced x-ray output when a calcite crystal was set for anomalous transmission. In that case, the fluorescence was the result of a nuclear n-γ reaction.

ACKNOWLEDGMENTS

The author wishes to acknowledge the able experimental assistance of L. D. Fullerton. The computer programming was performed by Mrs. E. Sonnenblick, whose understanding of the nature of the problem made for an effective interplay between the computer and the experiment.

[10] J. W. Knowles, Acta Cryst. 9, 61 (1956).